

## **Optical Pressure Measurements of Explosions**

**by Kevin L. McNesby, Matthew M. Biss, Richard A. Benjamin,  
and Ronnie A. Thompson**

**ARL-TR-6488**

**September 2013**

## **NOTICES**

### **Disclaimers**

The findings in this report are not to be construed as an official Department of the Army position unless so designated by other authorized documents.

Citation of manufacturer's or trade names does not constitute an official endorsement or approval of the use thereof.

Destroy this report when it is no longer needed. Do not return it to the originator.

# **Army Research Laboratory**

Aberdeen Proving Ground, MD 21005-5066

---

---

**ARL-TR-6488**

**September 2013**

---

## **Optical Pressure Measurements of Explosions**

**Kevin L. McNesby, Matthew M. Biss, and Richard A. Benjamin,  
Weapons and Materials Research Directorate, ARL**

**Ronnie A. Thompson  
Dynamic Science, Inc.**

<b>REPORT DOCUMENTATION PAGE</b>			<b>Form Approved OMB No. 0704-0188</b>	
<p>Public reporting burden for this collection of information is estimated to average 1 hour per response, including the time for reviewing instructions, searching existing data sources, gathering and maintaining the data needed, and completing and reviewing the collection information. Send comments regarding this burden estimate or any other aspect of this collection of information, including suggestions for reducing the burden, to Department of Defense, Washington Headquarters Services, Directorate for Information Operations and Reports (0704-0188), 1215 Jefferson Davis Highway, Suite 1204, Arlington, VA 22202-4302. Respondents should be aware that notwithstanding any other provision of law, no person shall be subject to any penalty for failing to comply with a collection of information if it does not display a currently valid OMB control number.</p> <p><b>PLEASE DO NOT RETURN YOUR FORM TO THE ABOVE ADDRESS.</b></p>				
<b>1. REPORT DATE (DD-MM-YYYY)</b>		<b>2. REPORT TYPE</b>		<b>3. DATES COVERED (From - To)</b>
September 2013		Final		January 2011–January 2013
<b>4. TITLE AND SUBTITLE</b>				<b>5a. CONTRACT NUMBER</b>
Optical Pressure Measurements of Explosions				<b>5b. GRANT NUMBER</b>
				<b>5c. PROGRAM ELEMENT NUMBER</b>
<b>6. AUTHOR(S)</b>				<b>5d. PROJECT NUMBER</b>
Kevin L. McNesby, Matthew M. Biss, Richard A. Benjamin, and Ronnie A. Thompson*				FY13AEET
				<b>5e. TASK NUMBER</b>
				<b>5f. WORK UNIT NUMBER</b>
<b>7. PERFORMING ORGANIZATION NAME(S) AND ADDRESS(ES)</b>				<b>8. PERFORMING ORGANIZATION REPORT NUMBER</b>
U.S. Army Research Laboratory ATTN: RDRL-WML-C Aberdeen Proving Ground, MD 21005-5066				ARL-TR-6488
<b>9. SPONSORING/MONITORING AGENCY NAME(S) AND ADDRESS(ES)</b>				<b>10. SPONSOR/MONITOR'S ACRONYM(S)</b>
				<b>11. SPONSOR/MONITOR'S REPORT NUMBER(S)</b>
<b>12. DISTRIBUTION/AVAILABILITY STATEMENT</b>				
Approved for public release; distribution is unlimited.				
<b>13. SUPPLEMENTARY NOTES</b>				
*Dynamic Science, Inc., 1003 Old Philadelphia Rd, Aberdeen, MD 21001				
<b>14. ABSTRACT</b>				
High-speed video and streak-camera imaging are used to measure peak pressures for explosions of spherical charges of C-4. The technique measures the velocity of the air shock produced by the detonation of the explosive charges, converts this velocity to a Mach number, and uses the Mach number to determine a peak shock pressure. Peak pressure measurements are reported from a few millimeters to ~1 m from the charge surface. Optical peak pressure measurements are compared to peak pressures measured using mechanical pressure transducers, and to peak pressure measurements estimated using the blast estimator computer code CONWEP. A discussion of accuracy of peak pressures determined optically is provided.				
<b>15. SUBJECT TERMS</b>				
explosions, pressure measurements, near field, high-speed imaging				
<b>16. SECURITY CLASSIFICATION OF:</b>			<b>17. LIMITATION OF ABSTRACT</b>	<b>18. NUMBER OF PAGES</b>
<b>a. REPORT</b>	<b>b. ABSTRACT</b>	<b>c. THIS PAGE</b>	UU	20
Unclassified	Unclassified	Unclassified		
				<b>19a. NAME OF RESPONSIBLE PERSON</b>
				Kevin L. McNesby
				<b>19b. TELEPHONE NUMBER (Include area code)</b>
				410-306-1383-

---

## Contents

---

<b>List of Figures</b>	<b>iv</b>
<b>1. Introduction</b>	<b>1</b>
<b>2. Background</b>	<b>1</b>
<b>3. Approach</b>	<b>3</b>
<b>4. Experimental</b>	<b>6</b>
<b>5. Results: Streak-Camera Rig</b>	<b>8</b>
<b>6. Results – Framing Camera</b>	<b>10</b>
<b>7. Summary and Conclusions</b>	<b>11</b>
<b>8. References</b>	<b>12</b>
<b>Distribution List</b>	<b>13</b>

---

## List of Figures

---

Figure 1. The evolution of the explosive near field. ....	2
Figure 2. A thermochemical calculation of detonation product gases for TNT/AL composite explosive—varying Al reactivity. ....	2
Figure 3. Several images (300-ns exposure) of the explosive near field for 450-g C-4 sphere. ....	4
Figure 4. Shock overpressure calculation schematic. ....	4
Figure 5. A comparison of optical and mechanical peak shock pressure measurements in the explosive mid-field for several TNT charges. ....	5
Figure 6. Error in optically based peak pressure measurements at higher Mach number (higher blast loading) when using the ideal gas assumption in Rankine-Hugoniot theory. ....	6
Figure 7. A 450-g C-4 sphere positioned within an indoor blast chamber at the ARL for one of the tests described here. ....	7
Figure 8. Photo and schematic of the streak camera rig, which employed a Photron SA-5 framing camera with the chip addressed to $8 \times 768$ pixels. ....	7
Figure 9. Peak shock pressures calculated using data from the streak-camera rig employing a direct numerical differentiation, and results calculated using the blast peak pressure simulator CONWEP. ....	8
Figure 10. The best-fit third-order polynomial to a set of streak-camera data for 450-g spherical C-4 charges. ....	9
Figure 11. Peak shock pressure based upon the numerical fit to data shown in figure 10. The disagreement is most severe at pressures above $\sim 25,000$ KPa. ....	9
Figure 12. Peak shock pressure and position vs. time for spherical C-4 charges. Measured using the Cordin Model 570 camera. ....	10
Figure 13. Optically based peak shock pressure measurements using the framing camera (Cordin Model 570) and the streak-camera rig, and predictions based upon CONWEP. Error is believed to be within 10% of actual, with the largest source of error being the exposure duration of each camera. ....	11

---

## 1. Introduction

---

The explosive near field for detonating high explosives is poorly defined. Most often, the explosive near field is given as covering the distance from the charge center of mass to a distance of many charge initial diameters, and/or covering the time from  $t = 0$  to the time when the leading shock separates from the detonation product gases, or in more strict regimes, covering the time from  $t = 0$  to the time when the detonation product gases reach a fixed composition “freeze out” prior to mixing with ambient air (1).

This region is often overlooked from an experimental point of view because the destructive nature of the environment in the explosive near field makes measurement difficult. Specifically, peak pressure and impulse measurements in the explosive near field are expensive and often suffer from poor repeatability because of gauge thermal effects, the need for fast gauge response, and the tendency for transducer-type gauges to exhibit degradation in performance with repeated exposure to high blast loadings (2).

Experience indicates that the most important information regarding blast performance of explosives is available exclusively in the near field. Since virtually all explosives exhibit some degree of non-ideality (3), the rate of detonation product expansion, temperature, and finite rate chemistry that occurs in the explosive near field determines all effects demonstrated downrange. Any ability to tailor energy delivery on target, to alter explosive impulse, peak shock, and thermal effect, is determined by the chemistry that occurs in the near field. This effect is most important for metallized explosives. The release of energy by metallized explosives, and how this energy release may alter the chemical makeup of detonation product gases has a significant effect on energy deposition on target (4). This report describes one aspect of quantifying the peak shock pressure in the explosive near field.

---

## 2. Background

---

Figure 1 shows a sequence of laser-illuminated shadowgraphs illustrating the evolution of the explosive near field for a 2-kg charge of TNT (trinitrotoluene,  $C_6H_2(NO_2)_3CH_3$ ) (4). In this figure, the near field is defined (somewhat arbitrarily) as the time from detonation to the time when the shock leaves the detonation products, shown in figure 1 as the fourth image from top, labelled as occurring for this test at 391  $\mu s$  after initiation. For many explosives, it is during this time that chemical reactions (mostly anaerobic), occurring within the detonation product gases, can influence the leading shock. Therefore, it is during this time that chemical tuning of the explosive for post-detonation performance must occur. For example, figure 2 shows a thermochemical calculation (5) of detonation product gas distribution for a TNT/Al mixture

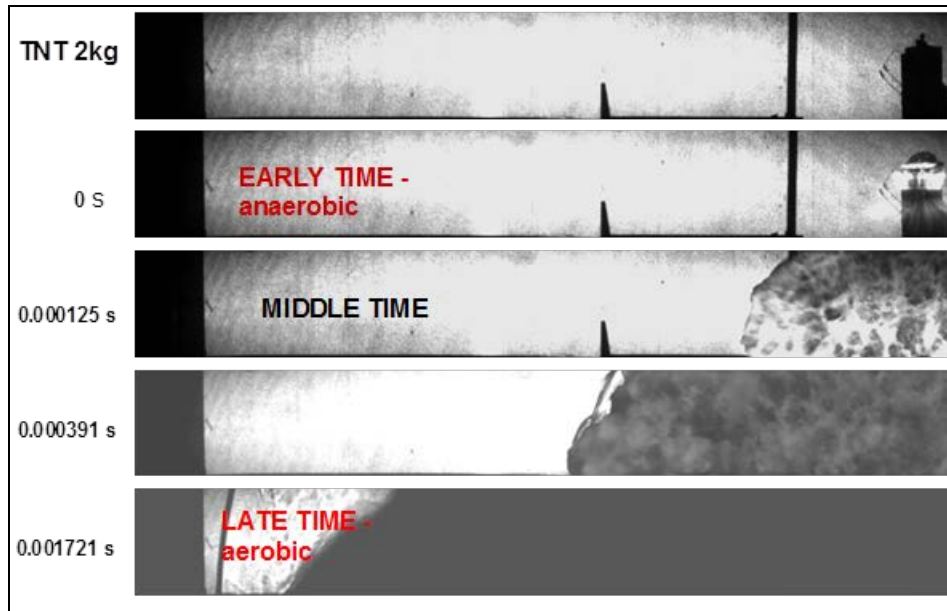


Figure 1. The evolution of the explosive near field.

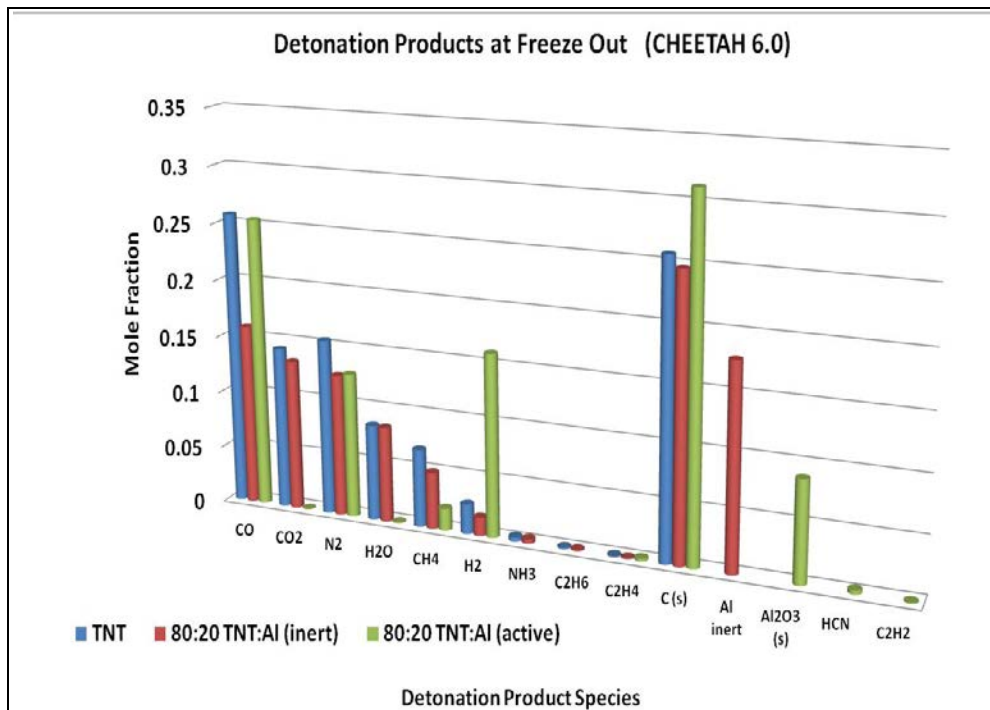


Figure 2. A thermochemical calculation of detonation product gases for TNT/AL composite explosive—varying Al reactivity.

(80:20 by weight), where the Al has been made inert, or fully reactive. The significance here is that early Al participation in the near field chemistry of the detonation product gases alters their makeup, relative to the case of addition of non-reactive Al. Figure 2 shows that the most significant change due to early Al reactivity is increased H<sub>2</sub> gas in the near-field detonation

product gases. It has been shown previously that addition of H<sub>2</sub> gas to near field detonation product gases can have a significant effect upon afterburn ignition times (4). The implication being that afterburning times can be tuned to bring detonation product afterburning into proximity of the leading shock, influencing brisance, and explosive impulse on target.

---

### 3. Approach

---

As previously described, real tuning of explosives for post-detonation performance will ideally measure output power in the explosive near field. The approach used in what follows concentrates on measurements of the peak shock pressures in real time for exploding, center detonated, 450-g spheres of Composition C-4 (92% trimethylenetrinitramine, RDX, C<sub>3</sub>H<sub>6</sub>N<sub>6</sub>O<sub>6</sub>, milspec). Figure 3 shows a sequence of high-speed framing camera images (2.5 million frames per second [Mfps], 300-ns exposure duration) of center-detonated C-4 spheres. A thermochemical calculation (5) indicates that detonation product gas species cease to change in composition when the detonation product gases for C-4 have expanded to approximately twice their initial volume. For the four frames shown in figure 3, the change in volume across the four frames is approximately a factor of 19. The approach used here relies on an analysis of high-speed images of the type shown in figure 3, obtained with a framing camera and with streak-camera techniques, to measure optically in one shot the peak shock pressures of exploding C-4 in the near field.

The method of determining shock peak pressures from shock velocities in air is based upon Rankine-Hugoniot theory and may be found in texts on the topic (6). The equations used here are developed using normal (planar) shocks, but are a reasonable approximation for the spherical shocks produced by the C-4 explosions because of the narrow thickness of the shock front (6). Figure 4 is a schematic of a gas travelling through a stationary shock front. In this model, supersonic gas at ambient pressure  $p_x$  at flow velocity  $u_x$  enters normal to the shock plane. At the shock plane the gas is decelerated to velocity  $u_y$  and compressed to pressure  $p_y$ . According to Rankine-Hugoniot theory, the shock overpressure,  $P$ , is given by:

$$P = [(7M_x^2 - 1)/6]p_x, \quad (1)$$

where  $M_x$  is the Mach number corresponding to the flow velocity of gas (air) entering the shock plane (6). The approach employed here is to assume the leading shock is at the surface of the expanding detonation product gases (1). High-speed imaging (framing and streak cameras) is used to measure position of the edge of the detonation product gases, and to measure shock velocities, convert the measured shock velocities to Mach number, and use equation 1 to calculate peak shock overpressures. This approach has been previously employed by the U.S. Army Research Laboratory (ARL) (1) to measure peak shock overpressures in the explosive mid-field (see figure 1, "Late Time") for TNT charges.

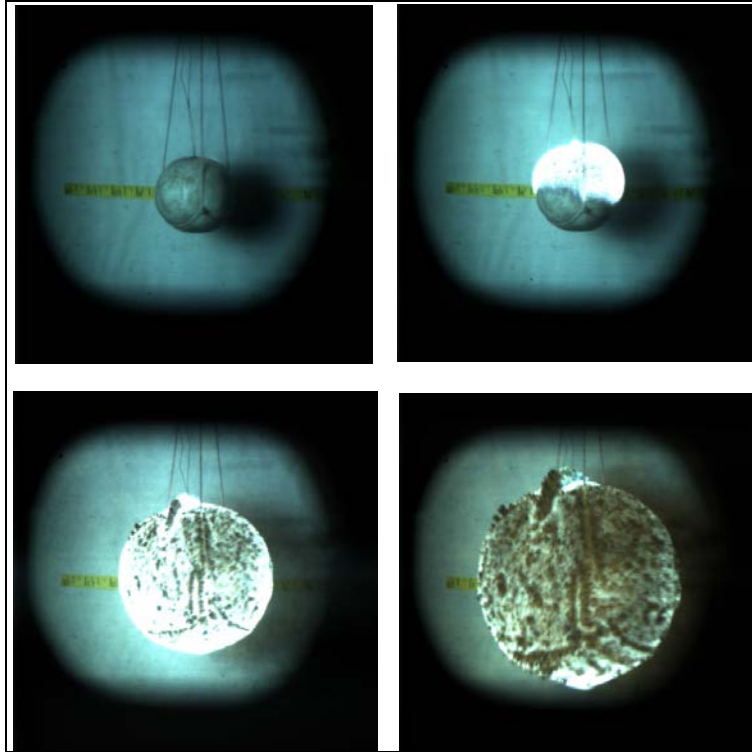


Figure 3. Several images (300-ns exposure) of the explosive near field for 450-g C-4 sphere.

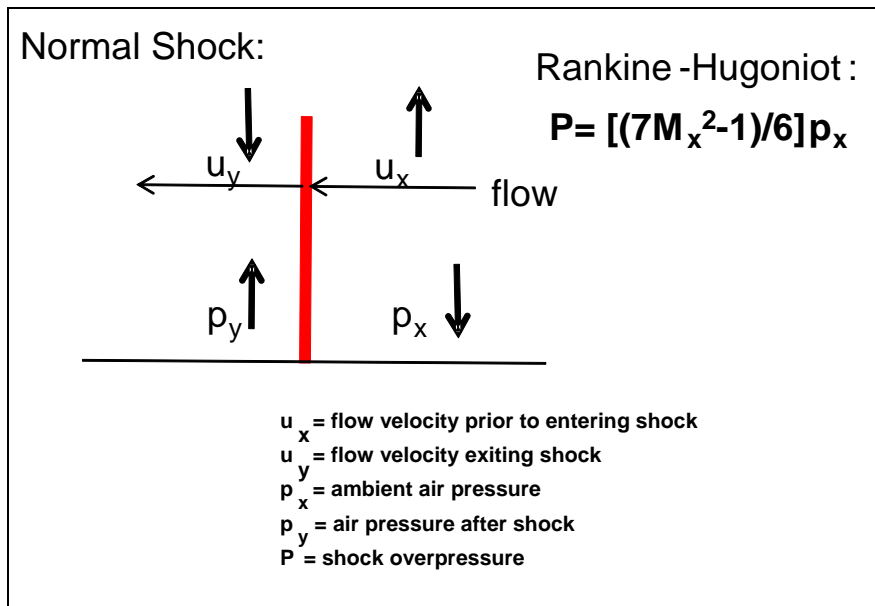


Figure 4. Shock overpressure calculation schematic.

A comparison of peak pressures measured using piezo-electric transducers (PCB, pencil-type) and using equation 1 is shown in figure 5 for the explosive mid-field. For each test, the optical method yields a considerably higher peak pressure. This is presumed to be caused by the actuation required by the mechanical transducer. For the explosive near-field measurements described here, Mach numbers higher than  $\sim 10$  require a modification to the Rankine-Hugoniot formulation shown in equation 1, necessary because at these higher blast loadings the perfect gas assumption for air is not accurate (7). Figure 6 shows a comparison of optically based peak shock pressure measurements for perfect and imperfect gases. At the higher Mach numbers encountered for near-field measurements, figure 6 shows error associated with use of equation 1 may approach 10%.

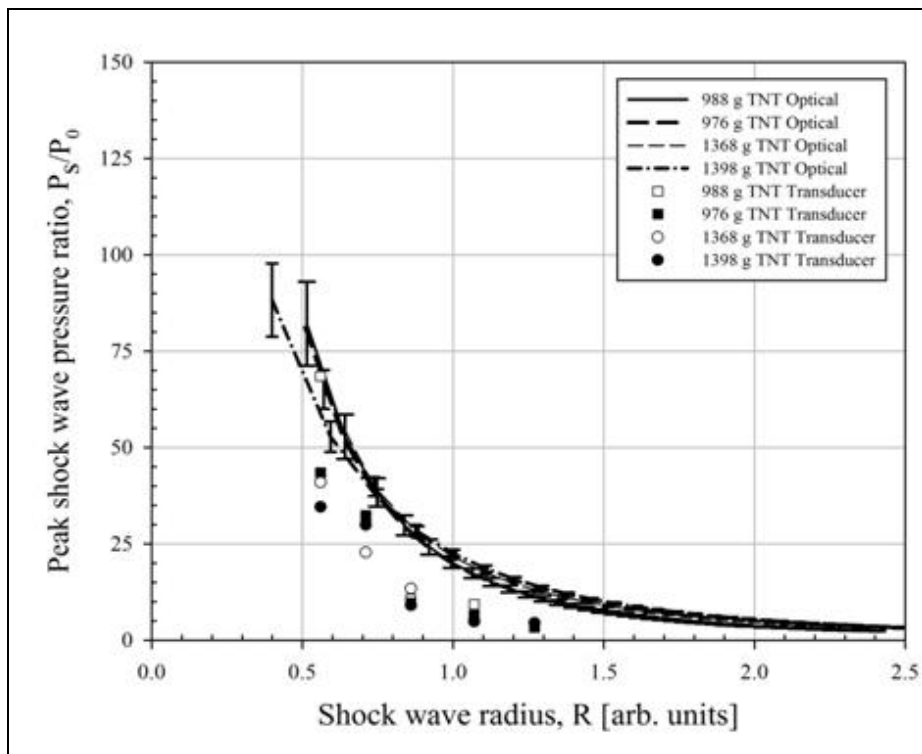


Figure 5. A comparison of optical and mechanical peak shock pressure measurements in the explosive mid-field for several TNT charges.

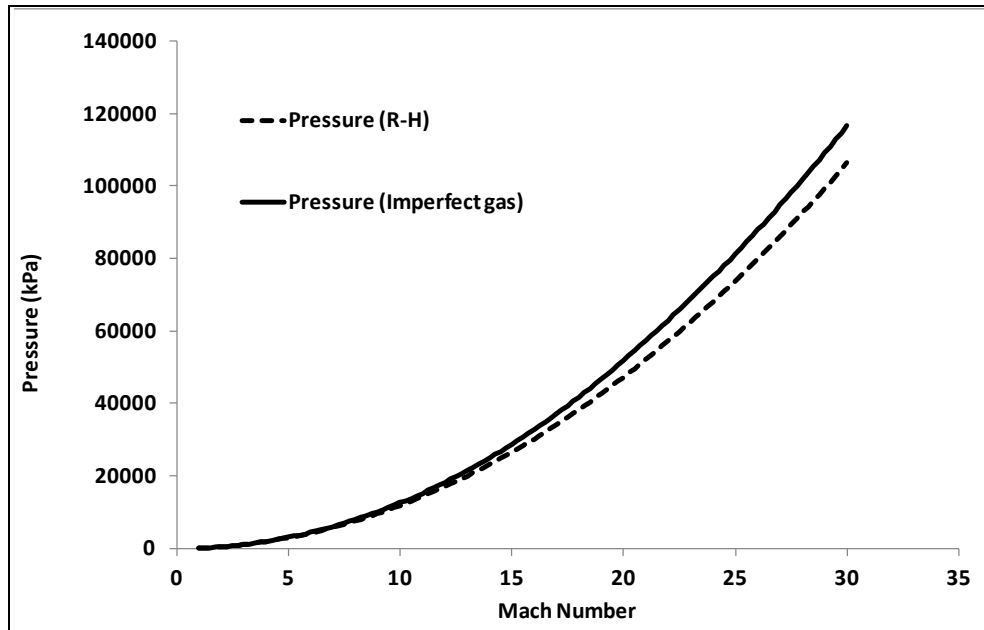


Figure 6. Error in optically based peak pressure measurements at higher Mach number (higher blast loading) when using the ideal gas assumption in Rankine-Hugoniot theory.

---

## 4. Experimental

---

Figure 7 shows a photograph of a C-4 sphere (450 g) positioned within an indoor blast chamber at ARL's facility located at Aberdeen Proving Ground, MD. The C-4 sphere was center detonated (RP-83 detonator). A mirror positioned above the charge provided a non-direct line of sight for streak-camera imaging. For framing camera imaging, a direct line of sight was employed. Figure 7 also shows a transducer-equipped blast wall and a blast bar gauge used to measure pressure for these experiments. Results from the blast wall and bar gauge diagnostics are not reported here.

The streak camera method was somewhat unique in that an addressable digital framing camera (Photron SA-5) was used. By defining the active pixel area to be  $8 \times 768$  pixels, streak-type images were obtained at 700,000 fps at an exposure time of 370 ns. For each shot the maximum number of frames was many thousands, exceeding the number required to image the gases and leading shock within the field of view. Figure 8 shows a photo and schematic of this setup. A speckled backing board placed immediately behind the focal plane of the camera provided contrast to enable visualization of the leading edge of the explosive gases and the point at which the leading shock separated from these gases.



Figure 7. A 450-g C-4 sphere positioned within an indoor blast chamber at the ARL for one of the tests described here.

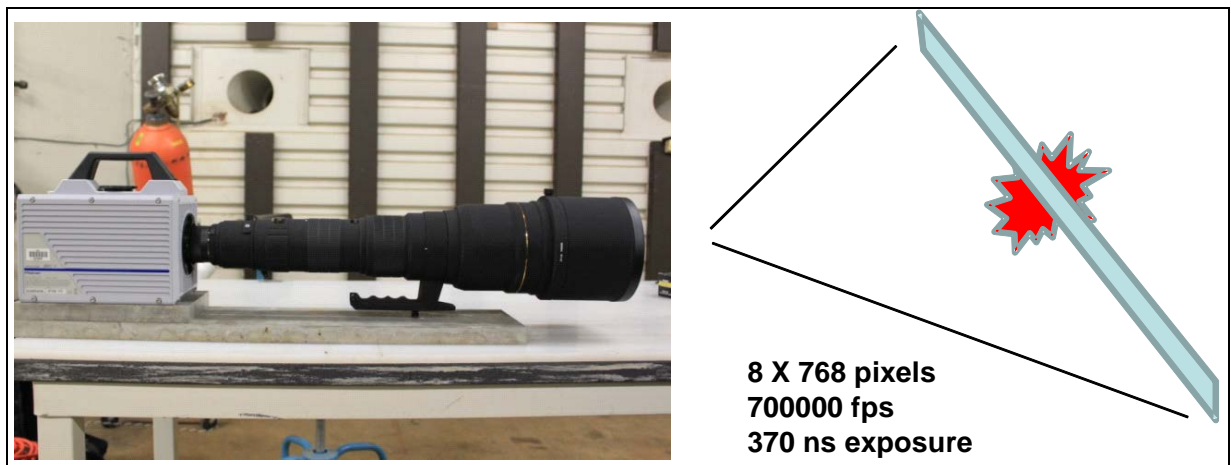


Figure 8. Photo and schematic of the streak camera rig, which employed a Photron SA-5 framing camera with the chip addressed to  $8 \times 768$  pixels.

Framing camera images were obtained using a Cordin Co. Model 570 digital framing camera operating at 2.5 Mfps, with an exposure time of 300 ns. Each recorded image was 4 megapixels in size. For each shot, the maximum number of frames was 74. An example of the output from this camera is shown in figure 3.

The experimental protocol was to use the streak-camera rig (Photron SA5) to record images from the charge over the entire explosive near field, and use the faster framing camera (Cordin 570) for measurements of the explosive near field immediately adjacent to the charge, where the gas expansion velocity was highest.

---

## 5. Results: Streak-Camera Rig

---

For the streak-camera measurements, each record was analyzed using the Photron PFV software. Prior to each shot, a test image was obtained with a meter stick positioned at the focal plane of the camera. From this image, a calibration of millimeters per pixel was obtained, and used in the analysis of the experimental data. In the Photron software, the position of the leading edge of the detonation product gases was given a pixel location, which was converted to a distance from charge center in millimeters. Resolution was  $\sim 1.35$  mm per pixel. Consecutive images were used to determine distance per unit time, and a peak pressure calculated based upon Mach number from measured shock velocities. Figure 9 shows the result of peak shock pressures calculated using data from the streak-camera rig employing a direct numerical differentiation, and results calculated using the blast peak pressure simulator CONWEP (8). Agreement is reasonable over all, but is poor in regions of high peak pressure/high Mach number. This disagreement at high pressure/Mach number is likely due to the framing rate of the streak camera rig being limited to 700,000 fps.

In an attempt to minimize the noise inherent in a direct numerical differentiation of the streak data, a third-order polynomial was fit to raw distance-vs.-time data (figure 10), and the best-fit equation was then differentiated to provide a smoother velocity-vs.-time record. This is shown in figure 11. As with the results of direct numerical differentiation, the results agree best with CONWEP predictions at peak pressures below  $\sim 20,000$  kPa (3000 psi).

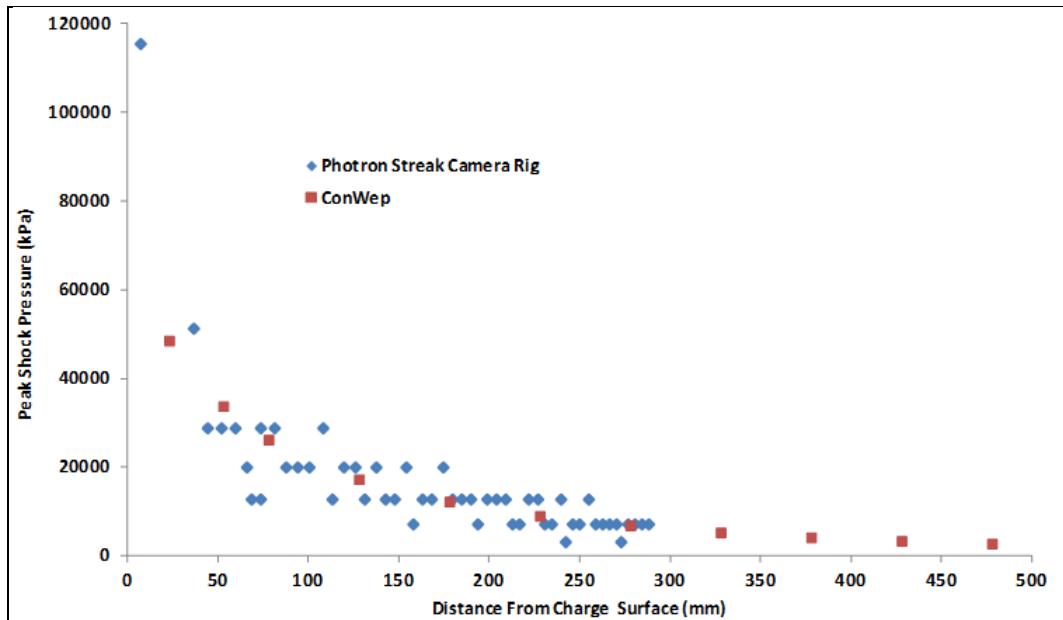


Figure 9. Peak shock pressures calculated using data from the streak-camera rig employing a direct numerical differentiation, and results calculated using the blast peak pressure simulator CONWEP.

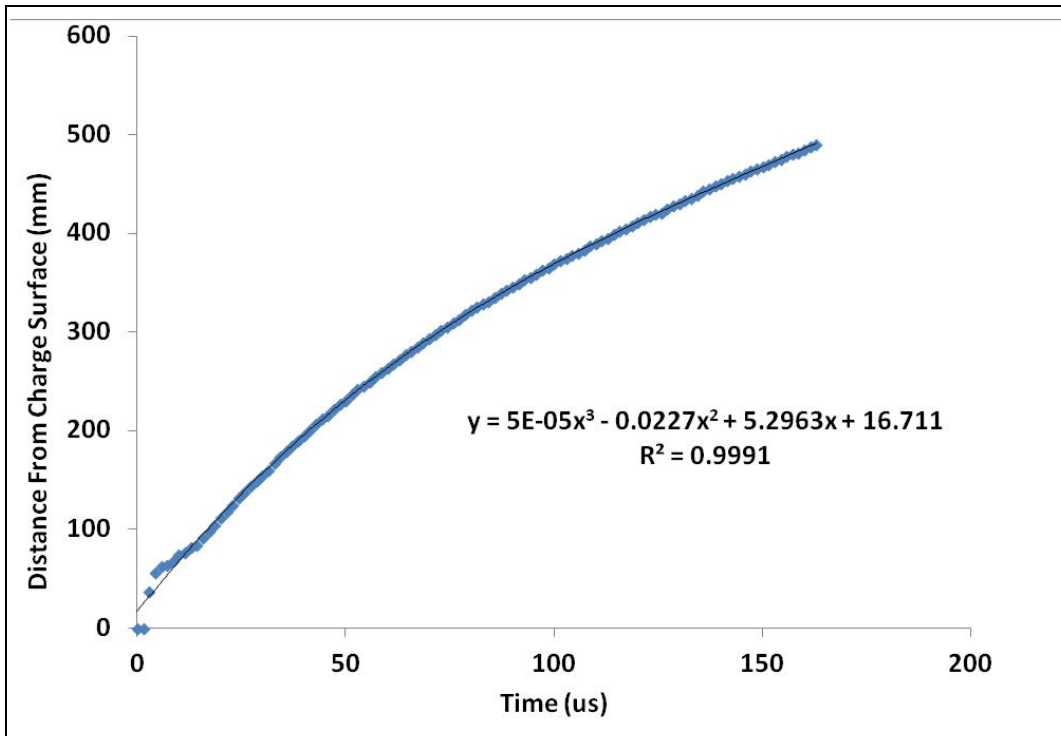


Figure 10. The best-fit third-order polynomial to a set of streak-camera data for 450-g spherical C-4 charges.

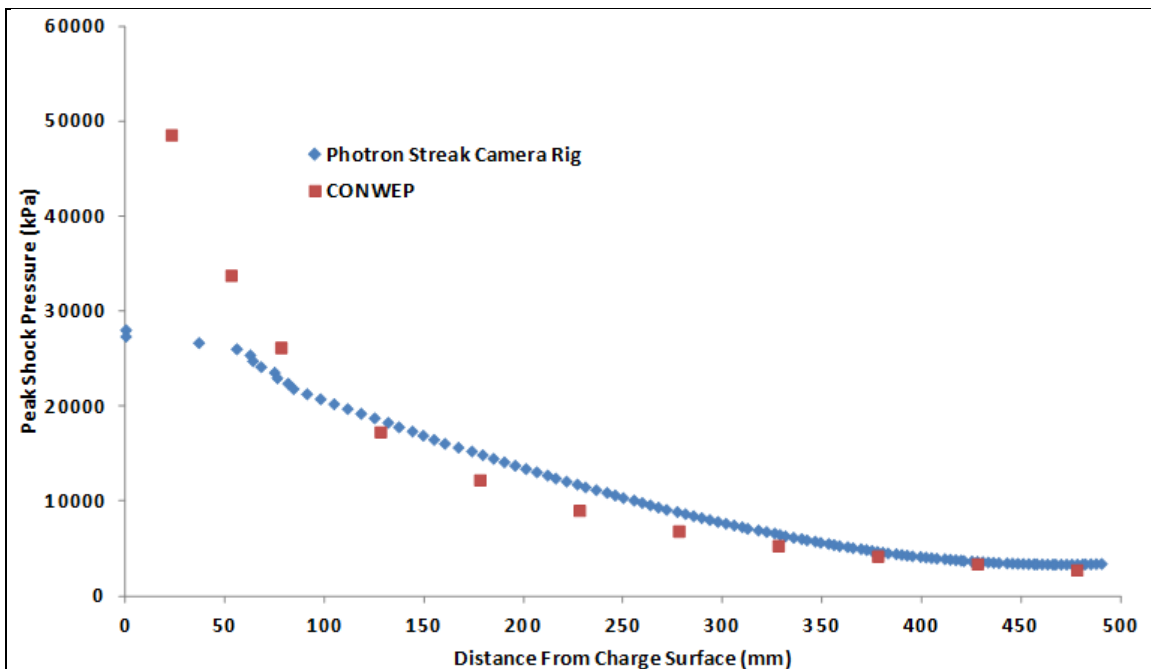


Figure 11. Peak shock pressure based upon the numerical fit to data shown in figure 10. The disagreement is most severe at pressures above ~25,000 KPa.

---

## 6. Results – Framing Camera

---

Framing camera (Cordin Model 570) images were recorded in a direct line of sight. Consecutive images were analyzed similar to methods employed for the streak camera images, using the Photron PFV software. Figure 12 shows leading shock position and differentiation of a best fit to position data resulting in a peak pressure vs. distance for a C-4 sphere similar to the spheres used in the streak camera measurements. It is worth noting that, although the C-4 spheres were prepared using hemispherical molds, the malleable nature of the C-4 caused each sample to vary in sphericity. The line of sight along which the framing camera data was analyzed was chosen to coincide with that used for the streak-camera data. Physical limitations of mirror placement prevented the simultaneous use of the two cameras. Figure 12 shows that the higher framing rate of the Cordin camera relative to the streak-camera rig ( $\sim 3.5\times$ ) provides data in reasonable agreement to CONWEP at distances immediately adjacent to the charge. Figure 13 shows the results of both measurements of optically based peak shock pressure and predictions based upon CONWEP. The results overall are in reasonable agreement with CONWEP predictions. Error in the measurements is believed to be less than 10%, with the main source of error being the duration of exposure for each camera.

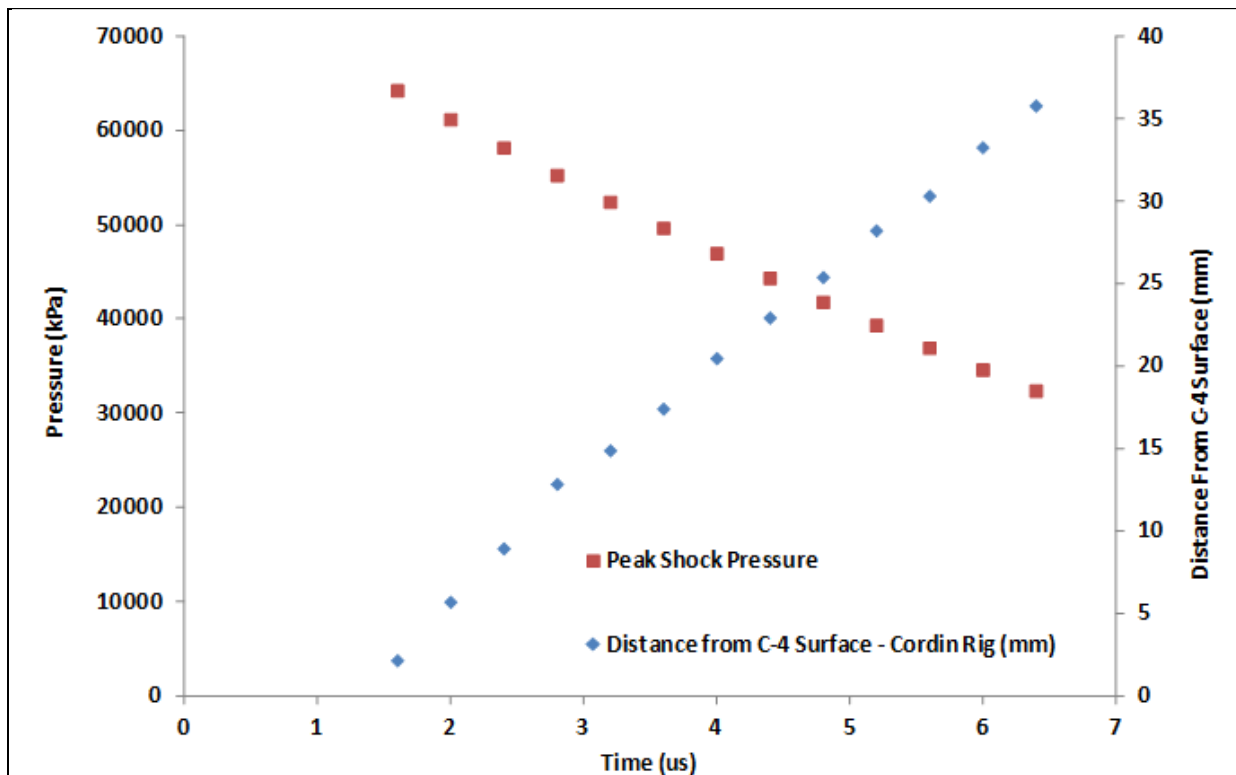


Figure 12. Peak shock pressure and position vs. time for spherical C-4 charges. Measured using the Cordin Model 570 camera.

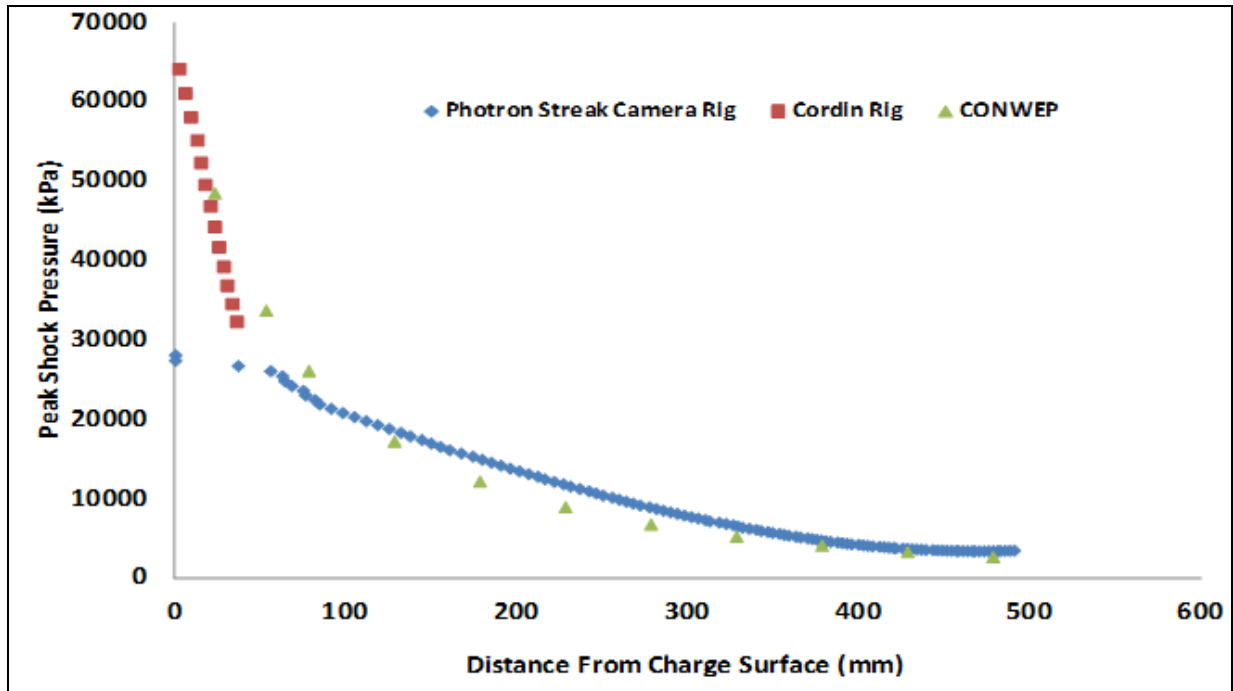


Figure 13. Optically based peak shock pressure measurements using the framing camera (Cordin Model 570) and the streak-camera rig, and predictions based upon CONWEP. Error is believed to be within 10% of actual, with the largest source of error being the exposure duration of each camera.

## 7. Summary and Conclusions

The results shown here indicate that high-speed, high-fidelity imaging (framing rates greater than 1 MHz at resolution approaching high definition) can make a significant contribution to analysis of the near-field behaviour of high explosives. For extremely high-fidelity records, direct numerical differentiation of position versus time data may be possible, but for noisy data (e.g., figure 12) a fit to position data, followed by differentiation of the resulting equation, yields smoother data for measurements reported here. However, fitment of position versus time data to a physically realistic function (e.g., Friedlander equation [6]) may also be useful. A real possibility here, and currently under pursuit by us in another test series, is the use of high-fidelity imaging to create pressure maps, providing a full cross section of the near-field explosive behaviour in a single test. ARL is currently pursuing an extension of this technique to create temperature and chemical species maps in the explosive near field.

---

## 8. References

---

1. McNesby, K. L.; Homan, B. E.; Lottero, R. E. *High Brightness Imaging for Real Time Measurement of Shock, Particle, and Combustion Fronts Produced by Enhanced Blast Explosives*; ARL-TR-3411; U.S. Army Research Laboratory: Aberdeen Proving Ground, MD, January 2005.
2. Walter, P. L. *Introduction to Air Blast Measurements*. PCB Technical Note TN-12; www.pcb.com.
3. Mader, C. L. *Numerical Modeling Off Explosives and Propellants*, 3rd ed.; CRC Press: Boca Raton, FL, 2008.
4. McNesby, K. L.; Homan, B. E.; Ritter, J. J.; Quine, Z.; Ehlers, R. Z.; McAndrew, B. A. Afterburn Ignition Delay and Shock Augmentation in Fuel Rich Solid Explosives. *Propellants, Explosives, Pyrotechnics* **2010**, *35* (1), 57–65.
5. Cheetah 6.0. Lawrence Livermore National Laboratory, 7000 East Ave., Livermore, CA 94550.
6. Kinney, G. F.; Graham, K. J. *Explosive Shocks in Air*, 2nd ed.; Springer-Verlag: Berlin, Germany, 1985.
7. Anderson, J. D. *Hypersonic and High Temperature Gas Dynamics*, 2nd Ed.; AIAA Education, 1996.
8. Hyde, D. *User's Guide for Microcomputer Programs: CONWEP and FUNPRO – Applications of TM 5-855-1*; U.S. Army Engineer Waterways Experimental Station, Vicksburg, 1988.

<u>NO. OF COPIES</u>	<u>ORGANIZATION</u>
1 (PDF)	DEFENSE TECHNICAL INFORMATION CTR DTIC OCA
1 (PDF)	DIRECTOR US ARMY RESEARCH LAB IMAL HRA
1 (PDF)	DIRECTOR US ARMY RESEARCH LAB RDRL CIO LL
1 (PDF)	GOVT PRINTG OFC A MALHOTRA
2 (PDF)	US ARMY RSRCH OFC AMSRD ARL RO P R ANTHENIEN J PARKER
1 (PDF)	DARPA/DSO J GOLDWASSER
2 (PDF)	US ARMY AMRDEC AMSRD AMR PS PT J NEIDERT P JOHNS
1 (PDF)	US ARMY ARDEC AMSRD AAR AEE W R DAMAVARAPU
1 (PDF)	US ARMY ARDEC AMSRD AAR AEE W E BAKER
1 (PDF)	US ARMY ARDEC AMSRD AAR MEE W S NICOLICH
1 (PDF)	US ARMY ARDEC AMSRD AAR AEE W E CARAVACA
2 (PDF)	US ARMY ARDEC RDAR MEE W J O'REILLY W BALAS-HUMMERS
1 (PDF)	US ARMY ARDEC RDAR MEF E D CARLUCCI

<u>NO. OF COPIES</u>	<u>ORGANIZATION</u>
1 (PDF)	US ARMY PEO AMMO SFAE AMO CAS P MANZ
1 (PDF)	OFC OF NAVAL RSRCH C BEDFORD
1 (PDF)	DTRA B WILSON
<u>ABERDEEN PROVING GROUND</u>	
31 (PDF)	DIR USARL RDRL CIO LA T LANDFRIED RDRL WML M ZOLTOSKI RDRL WML A F DE LUCIA W OBERLE RDRL WML B J GOTTFRIED J CIEZAK-JENKINS J MORRIS B RICE W MATTSON R PESCE-RODRIGUEZ R SAUSA N TRIVEDI I BATYREV S BUNTE RDRL WML C K MCNESBY K SPANGLER B ROOS E BUKOWSKI S AUBERT M BISS RDRL WML D R BEYER RDRL WML E P WEINACHT RDRL WML F T BROWN RDRL WML G W DRYSDALE RDRL WML H J NEWILL RDRL WM P BAKER B FORCH P PLOSTINS RDRL WMM J ZABINSKI

NO. OF  
COPIES ORGANIZATION

RDRL WMP  
D LYON  
RDRL WMP A  
B RINGERS